Liquid Chromatography-Mass Spectrometry-based Metabolomics and Lipidomics Reveal Toxicological Mechanisms of Bisphenol F in Breast Cancer Xenografts

Zhao C. [1, 2], Xıe P. [3], Song Y. [1], Yang T. [1], Tang Z. [1], Xıang L. [1], Zhao H. [1], Wang H. [2], And Caı Z. [1, *]

[1]State Key Laboratory of Environmental and Biological Analysis, Department of Chemistry, Hong Kong Baptist University, Hong Kong SAR, China.

[2]State Key Laboratory of Environmental Chemistry and Ecotoxicology, Research Center for Eco-Environmental Sciences, Chinese Academy of Sciences, Beijing, China.

[3]Ministry of Education Key Laboratory of Analysis and Detection Technology for Food Safety, Fuzhou University, Fuzhou, China. *corresponding author: CAI Z. e-mail: zwcai@hkbu.edu.hk

Abstract. Bisphenol F (BPF) is a major alternative to bisphenol (BPA) and has been widely used. Although BPA exposure is known to generate various toxic effects, toxicity of BPF remains under-explored. A comprehensive method involving mass spectrometry (MS)-based global lipidomics and metabolomics, and matrix-assisted laser desorption/ionization-mass spectrometry (MALDI)-imaging MS (IMS) was used to study the toxic effects of BPF and the underlying mechanisms on breast cancer xenografts. Our results demonstrated that BPF exposure disturbed the metabolome and lipidome of kidney and liver without morphological alterations. BPF exposure induced the reprogramming of the glutathione (GSH) biosynthesis and glycolytic metabolism by activating glycine, serine, cysteine, glutamine, lactate and pyruvate although. It also perturbed the biosynthesis and degradation of glycerophospholipids (GPs) and glycerolipids (GLs), resulting in abnormality of membrane homeostasis and cellular functions. Moreover, the spatial distribution and profile of metabolites changed across the renal cortex and medulla regions after the BPF treatment. Levels of phosphatidylethanolamines (PE) and triacylglycerols (TAG) increased in renal medulla and pelvis, while the levels of phosphatidylcholines (PC) and phosphatidylinositols (PI) increased in renal cortex and pelvis. These observations offer a deeper understanding of the critical role of metabolites and lipid reprogramming in BPF-induced biological effects.

Keywords: Bisphenol F, Metabolomics, LC-MS/MS, MALDI-IMS, Breast cancer xenografts.

1. Introduction

As a very important alternative to bisohenol A (BPA), bisohenol F (BPF) is widely used in industrial and daily applications, such as water pipes, liners, adhesives, plastics, food packaging, dental sealants, and lacquers (Office of Environmental Health Hazard Assessment, 2012). Due to its widespread use, BPF has been detected in various matrices (Liao and Kannan, 2014).

There is increasing evidence suggesting that BPA as an endocrine disrupting chemical (EDC) might cause a series of adverse health effects. Exposure to BPA has been intimately linked with the incidence of certain tumors (Maffini *et al*., 2006), including breast cancers (Pupo *et al*., 2012). BPA used G protein-coupled receptor (GPER) to induce cell proliferation and chemoresistance in breast cancer cells (Lapensee *et al*., 2009). Previous investigations have demonstrated that prenatal exposure to BPA may have increased the risks of breast cancer (Maffini *et al*., 2006). In addition to direct activation of estrogen-dependent tumor cell growth, Lozada and Keri (2011) observed that exposure to BPA during different biological states of human breast cancer xenografts may increase mammary susceptibility depending on the changes of molecular mechanisms of fetal glands without morphological alterations.

Bisphenol F has estrogenic, androgenic, antiestrogenic and antiandrogenic activity similar to BPA (Rochester and Bolden, 2015). *In vitro*, BPF also displayed other biological effects, including DNA damage, cellular dysfunction and chromosomal aberrations (Cabaton *et al*., 2009). However, cytotoxicity effects and molecular mechanisms underlying the carcinogenesis of BPF *in vitro* and *in vivo* are still unclear, such as breast cancers.

Breast cancer is one of the most common malignancy in women worldwide. Liver, lung and kidney are the critical sites of cancer metastasis (Weigelt *et al*., 2005). Many studies showed that abnormal metabolism is one of the critical characteristics of breast tumor in cell experiments, whereas metabolic variations in breast tumor-bearing tissues remain elusive. Metabolomics and lipidomics in cancer provide important information on pathophysiology beyond genomics and proteomics data. Metabolomic profiling is widely used in the assessment of cancer development induced by environmental xenobiotics, and is a useful tool for identification and discovery of cancer biomarkers both *in vitro* and *in vivo* (McCarthy, 2012). In addition to changes in global metabolomics, revealing metabolites spatially *in situ* also contributes to

understanding tumor generation and tumor microenvironments in pathology and physiology. Matrix-assisted laser desorption/ ionization-mass spectrometry (MALDI)-imaging MS (IMS) has been used to identify various metabolites and profile their spatial distribution in tissue sections by a label-free method (Norris *et al*., 2013). Herein, for the first time, the established omics and IMS approach were utilized in the breast cancer xenografts to investigate the disorders and spatial distribution of BPF metabolites between kidney and liver.

(A) (B)

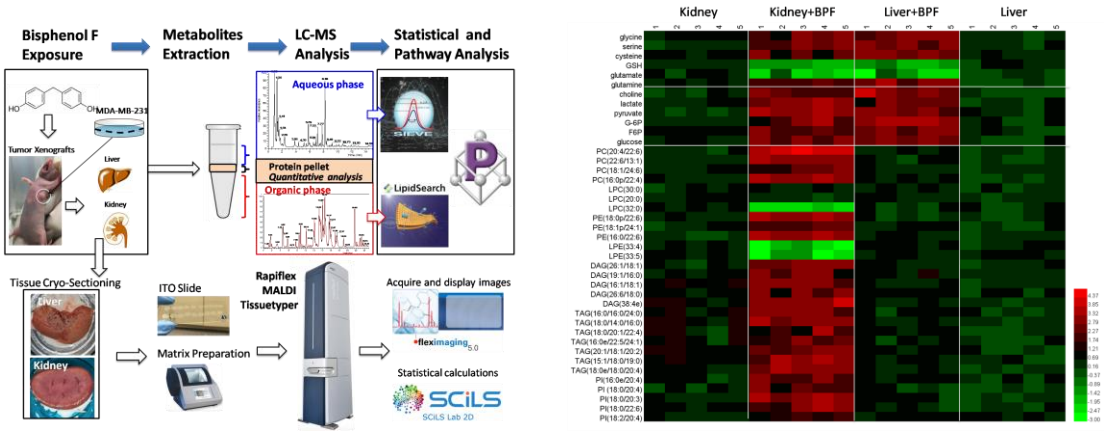

Figure 1. (A) Workflow of the method involving MS-based global lipidomics and metabolomics, and MALDI-IMS; (B) Heat map analysis of identified metabolites after BPF exposure. The metabolites are represented on the horizontal axis, the sample information is shown on the vertical axis, and the up- and down-regulated metabolites are indicated in red and green, respectively.

2. Materials and methods

2.1. Cell culture

MDA-MB-231 cell line (American Type Culture Collection) was maintained in culture medium including dulbecco's modified Eagle's medium (without phenol red) supplemented with 10% fetal bovine serum, 100 U/mL penicillin G and 100 U/mL streptomycin sulfate (Thermo Fisher Scientific, Waltham, MA, USA) in a humidified 37 °C incubator supplied with 5% CO_2. Cells were cultured until 80% confluence and were diluted to proper density by digestion with trypsin (Thermo Fisher Scientific).

2.2. Treatments and sample analysis

The tumor xenografts were carried out as described in Lozada and Keri (2011) with modifications. The details of animal experiments and metabolite extraction from tissues may be found in the Electronic Supplementary Material. The LC-MS/MS-based global metabolomics, quantitative analysis of extracted proteins and data processing were also carried out as described in Electronic Supplementary Material.

2.3 MALDI-IMS analysis

The kidney and liver were fixed by solid glue on the cutting stage. The tissues were sectioned at 14 μm thickness using a CryoStar Nx70 cryostat (Thermo Fisher Scientific, Walldorf, Germany) at -20 °C, and thaw-mounted onto ITO coated glass slides. The ITO-slide was dried in a vacuum desiccator for 20 min before matrix spraying. Solutions of NEDC for matrix and mixture standard solutions containing small molecules were prepared as described in Wang *et al*. (2014). The matrix was sprayed onto the sections mounted onto ITO-slides using an automatic matrix sprayer (ImagePrep, Bruker Daltonics, Billerica, MA) with the spraying protocol of Wang *et al*. (2014).

MALDI-IMS was carried out as described in Liu *et al*. (2017) with some modifications. In brief, the experiments were performed on an rapifleX^{TM} MALDI Tissuetyper^{TM} (Bruker Daltonics) equipped with a smartbeam^{TM} 3D laser in the single mode. The mass spectra data were acquired at a mass range of 200-1,100 m/z in the negative mode by averaging signal from 1,000 shots at 3.0 × 2810 volts detector gain and 30% laser power. The other parameters were optimized and fixed during the whole experiments, including a reflector voltage of 20.84 kV, a lens voltage of 11.00 kV, an ion source voltage of 20 kV, a pulsed ion extraction time of 100 ns, and the matrix suppression of 270 m/z. The spatial resolution for MALDI-IMS was acquired at 50 μm. The external mass calibration was performed before data acquisition. Four lipids (PE (38:4) $[M-H]^-$, 766.537 Da; PI (38:4) $[M-H]^-$, 885.549 Da; ST (d18:1/22:0) $[M-H]^-$, 878.602 Da; ST (d18:1/24:0) $[M-H]^-$, 906.633 Da) were selected as internal mass calibration in the linear mode to monitor the IMS performance. MALDI-IMS raw data and all ion images were first opened in flexImaging 5.0 software (Bruker Daltonics), and then analyzed, calibrated and imported into SCiLS Lab 2016a software. The standard processing pipeline was used for statistical analysis of IMS data, including segmentation, weak denoising, total ion count (TIC) normalization, principal component analysis (PCA) and partial least squares discriminant analysis (PLS-DA). At the same time, the LC-MS/MS data underwent multivariate pattern

recognition analysis by using SIMCA-P and LipidSearch software. The comparative results from LipidSearch, SIMCA-P and SCiLS Lab 2016a software served the purpose to complement and verify each analysis.

3. Results and discussion

3.1 Effect of BPF on breast cancer xenografts

The over-expression of epidermal growth factor receptor (EGFR) has been associated with some critical features of breast cancer generation, development and proliferation. Therefore, to investigate whether BPF may affect expression of EGFR in the MDA-MB-231 breast cancer xenografts, IRdye 800CW-EGF was selected for monitoring the tumor grow following BPF exposure using an *in vivo* near-infrared (NIR, 700-1000 nm) imaging method.

Representative NIR images of MDA-MB-231 xenografts at 4 d after injection of IRdye 800CW-EGF were shown in Figure S1A. NIR signal was visualized in the armpit tumor regions of each mouse. The results showed that only tumor weight and tumor volume increased significantly in the BPA and BPF groups compared with the control (Figure S1B and S1C). It can be seen that the tumor volumes in BPF- and BPA-treated groups increased significantly, by 70.0% and 65.7%, respectively (Figure S1B). The tumor weights in the olive oil (control), BPA- (100 μg /kg body weight /day) and BPF (100 μg /kg body weight/day) - treated groups were 0.3 ± 0.15 g, 0.60 ± 0.12 g, 0.56 ± 0.10 g, respectively (Figure S1C). Except the breast tumors, no significant BPF-induced variation was detected in the weight and histological analysis of liver and kidney as compared with the control ($P > 0.05$, data not shown). It may be concluded that BPF exposure may increase tumor proliferation of breast cancer xenografts through molecular alternation of tissues without associated morphological variations. The results indicated that the selected dose of BPF did not elicit any significant effect on kidney and liver, which was in agreement with previous studies (Lozada and Keri, 2011).

3.2 Omics analysis of BPF effects on tissue metabolic profiling

We developed a integrated workflow to realize accurate and exhaustive lipidomics and metabolomics profiles of tissue samples by combining LC-Orbitrap Fusion Tribird, Q Exactive focus orbitrap LC-MS/MS system and specialized software for automated identification of global lipids and metabolites (Figure 1A). The optimized protocol provided good reproducibility and sensitivity in one single liquid-liquid extraction. The strategy was applied and validated successfully in kidney and liver of breast cancer xenografts following the consecutive administration of BPF.

As shown in Figure S2, the PLS-DA score plots for positive and negative ionization modes revealed that all BPF-treated groups as well as the control groups showed distinct separations in the metabolomic and lipidomic profiles The potential biomarkers were identified and were shown in Table S2. From the heat map in Figure 1B, amino acids, glutathione (GSH)-related chemicals, glycolytic intermediates, lipids and other organic compunds displayed remakable variations in the breast cancer xenografts after BPF treatment.

When comparing liver samples between BPF-treated group and the control, the endogenous metabolites induced by BPF exposure displayed significant increases in glutamate, glutamine, GSH, glycine, serine, cysteine, G-6P, lactate, and pyruvate, but no remarkable variation in the biosynthesis and metabolism of lipids. For metabolomics analysis of kidney, the lipid metabolites showed a higher abundance in the BPF-treated group compared with the control, including phosphatidylcholines (PC), phosphatidylethanolamines (PE), phosphatidylinositols (PI), diacylglycerols (DAG) and triacylglycerols (TAG), and a lower abundance in lyso phosphatidylcholines (LPC) and lyso phosphatidylethanolamines (LPE). Similar to liver tissue, the GSH-related chemicals and glycolytic intermediates also increased significantly in kidney tissue. The results suggested that the lipidome and metabolome of kidney and liver were perturbed significantly after BPF exposure.

3.3 Pathways of BPF toxic effects on kidney and liver

Consistent with reported findings, the detected metabolites such as lactate, choline and lipids were closely associated with increased activity of tumor cell proliferation in breast cancers (Table S2). From extracts of liver and kidney, BPF exposure remarkably down-regulated GSH biosynthesis, including decreasing abundance of GSH, glutamate, glutathione synthetase (Gss), γ-glutamyl-transferase (Ggt) and glutaminase 2 (Gls2), as well as increased abundance of glycine, serine and glutamine (Table S1, S2; Figure 2A). Gss covalently links γ-glutamyl-cysteine and glycine to catalyze formation of GSH (Gorrini *et al*., 2013). The change in metabolite abundance was verified by decreased mRNA levels of Gss and Gls2 in the GSH biosynthesis. The results suggested that potential modulation of GSH biosynthesis was generated after BPF treatment in mouse kidney and liver, which is a critical pathway involved in the glycolysis, energy metabolism and tumor proliferation. Hassan *et al*. (2012) reported that BPA induced hepatotoxicity by generation of oxidative stress, following significant decreased levels of GSH and expression of antioxidant gene. Compared with BPA, BPF exposure also caused liver and kidney injury by disturbing the antioxidant defense system-related metabolites and enzymes (Table S2, Figure 2A), affecting the oxidant /antooxidant balance in breast cancer xenografts. It likely caused ROS generation, further induced oxidative damage by attacking cell membrane, DNA, RNA, and ultimately resulted in tissue damage (Kabuto *et al*., 2003).

(A) (B)

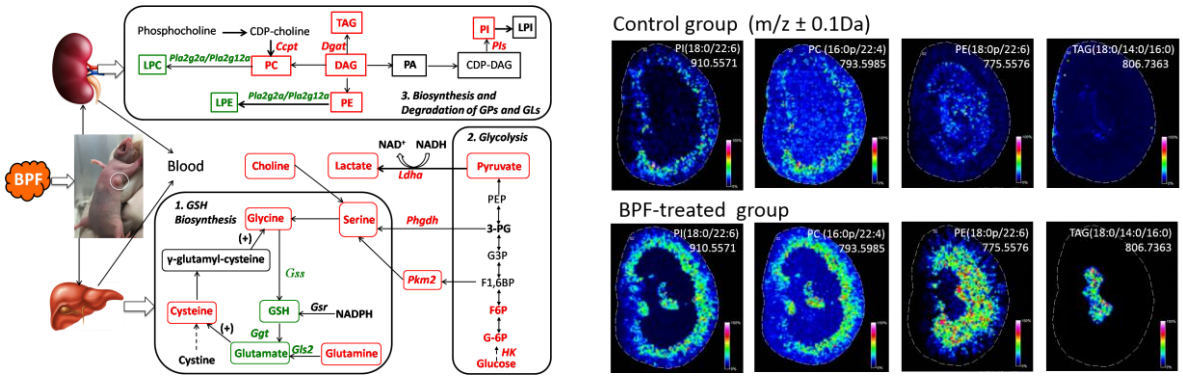

Figure 2. (A) BPF exposure in kidney and liver of breast cancer xenografts induced global metabolic disturbances in (1) GSH biosynthesis, (2) glycolysis and (3) biosynthesis and degradation of GPs and GLs. Up- and down-regulated metabolites and lipids are represented in red and green, respectively. (B) Representative ion images of lipid metabolites in a kidney section.

In liver and kidney tissues, the BPF-treated group differed with the former showing increased abundance of lactate, pyruvate, glycolytic intermediates (fructose-6-phosphate [F6P] and glucose-6-phosphate [G-6P]) and glucose in glycolysis. These results were validated by the elevated mRNA levels of hexokinase (HK), pyruvate kinase isozymes M2 (Pkm2), and lactate dehydrogenase A (Ldha) when the kidney was treated with BPF (Table S1). Overall, the up-regulated glycolysis promoted tumor proliferation, indicating that it is an important feature in the Warburg effect (Figure 2A). Our results suggested that BPF exposure reprogrammed the GSH biosynthesis and glycolytic metabolism, reflecting a possible metabolism disturbance in the metabolic process of BPF, and resulting in the tumor cell proliferation and tissue damage in breast cancers.

Lipid molecules play critical roles in the biological process of tumor growth. Alternations of lipid components in membrane can significantly affect the activity of membrane proteins that serve as receptors, ion channels and signal transducers, and further influence the cellular functions during cancer generation and transformation (Volmer *et al*., 2013). Therefore, the detection of tumor related-membrane lipid is essential in elucidating the characteristics of tumor. Previous studies indicated that variations of lipids determination may be involved in tumor progression in human cancers, such as breast cancers (Doria *et al*., 2012).

Glycerophospholipids (GPs) are considered as the major structural lipids and also the precursors of lipid mediators. It was found that PC and PE are the major components of cell membrane lipids, and contributed to cell division, cytokines secretion and cell proliferation. PI participate in vesicle formation and cell signaling, and are located on the cytoplasmic surface of the membrane (Escriba *et al*., 2008). In this study, the kidney samples with BPF treatment showed increased abundance of GPs (PC, PE and PI) and glycerolipids (GLs) (DAG and TAG) and decreased abundance of LPC and LPE, potentially demonstrating the functional variation of lipids in the membrance remodeling (Table S2, Figure 2A). The results were verified by increased mRNA levels of Ccpt, Dgat and PI, and decreased mRNA levels of Pla2g2a / Pla2g12a in the BPF-treated group as compared to the control (Table S1). BPF can induce the functional and structural variations of lipids via the synergistic regulation of essential enzymes and lipid metabolites. We also visualized the distribution pattern of different lipids in kidney by MALDI-IMS (Figure 2B). Different metabolites were distributed across the renal cortex and medulla regions. For the BPF-treated group, PE (such as PE (18:0p/22:6) m/z 775.5576) and TAG (such as TAG (18:0/14:0/16:0) m/z 806.7363) increased in renal medulla and pelvis, and PC (such as PC (16:0p/22:4) 793.5985) and PI (such as PI (18:0/22:6) m/z 910.5571) also increased in renal cortex and pelvis.

4. Conclusions

In summary, a simple method was developed and applied successfully for global lipids and metabolites fingerprinting of kidney and liver using LC-MS/MS and MALDI-IMS in BPF-treated breast cancer xenografts. The results indicated that MS-based metabolic profiling may directly reflect the metabolic variations caused by BPF, and provide novel insights into the relationship between chemical exposure and toxicological mechanisms in organisms. Lipids-based investigation may be therefore very useful for the diagnosis of breast cancers.

5. Acknowledgments

The work was supported by grants from the National Natural Science Foundation of China [grant number 21507106, 21505111, 91543202].

References

Cabaton, N., Dumont, C., Severin, I., Perdu. E., *et al.* (2009), Genotoxic and endocrine activities of bis (hydroxyphenyl) methane (BPF) and its derivatives in the HepG2 cell line, *Toxicology*, **255**, 15-24.

Doria, M. L., Cotrim, C. Z., Simões, C., Macedo, B., *et al.* (2013), Lipidomic analysis of phospholipids from human mammary epithelial and breast cancer cell lines, *Journal of Cellular Physiology*, **228**, 457-468.

Escribá, P. V., González-Ros, J. M., Goñi, F. M., Kinnunen, P. K., *et al.* (2008), Membranes: a meeting point for lipids,

proteins and therapies, *Journal of Cellular and Molecular Medicine*, **12**, 829-875.

Gorrini, C., Harris, I. S, Mak, T. W. (2013), Modulation of oxidative stress as an anticancer strategy, *Nature Reviews Drug Discovery*, **12**, 931-947.

Hassan, Z. K., Elobeid, M. A., Virk, P., Omer, S. A., *et al*. (2012), Bisphenol A induces hepatotoxicity through oxidative stress in rat model, *Oxidative Medicine and Cellular Longevity*, **2012**, doi:10.1155/2012/194829.

Kabuto, H., Hasuike, S., Minagawa, N., Shishibori, T. (2003), Effects of bisphenol A on the metabolisms of active oxygen species in mouse tissues, *Environmental Research*, **93**, 31-35.

Lapensee, E. W., Tuttle, T. R., Fox, S. R, Ben-Jonathan, N. (2009), Bisphenol A at low nanomolar doses confers chemoresistance in estrogen receptor-α-positive and -negative breast cancer cells, *Environmental Health Perspectives*, **117**,175-180.

Liao C., Kannan K. (2014), A survey of alkylphenols, bisphenols, and triclosan in personal care products from China and the United States, *Archives of Environmental Contamination and Toxicology*, **67**,50-59.

Liu, H. H., Li W., He Q., Xue J. J., *et al*. (2017), Mass spectrometry imaging of kidney tissue sections of rat subjected to unilateral ureteral obstruction, *Scientific Reports*, **7**, 41954. DOI: 10.1038/srep 41954.

Lozada, K. W., Keri, R. A. (2011), Bisphenol A ıncreases mammary cancer risk in two distinct mouse models of breast cancer, *Biology of reproductıon*, **85**, 490-497.

Maffini M. V., Rubin, B. S, Sonnenschein, C., Soto, A. M. (2006), Endocrine disruptors and reproductive health: the case of bisphenol A. *Molecular and Cellular Endocrinology*, **255**,179-186.

McCarthy, N. (2012), Metabolism: unmasking an oncometabolite, *Nature Reviews Cancer*, **12**, doi: 10.1038/nrc3248.

Norris, J. L., Caprioli, R. M. (2013), Analysis of tissue specimens by matrix-assisted laser desorption/ ionization imaging mass spectrometry in biological and clinical research, *Chemical Reviews*, **113**, 2309-2342.

Office of Environmental Health Hazard Assessment. (2012), Biomonitoring California: *p,p*'-Bisphenols and Diglycidyl Ethers of *p,p*'-Bisphenols.

Pupo, M., Pisano, A., Lappano, R., Santolla, M. F., *et al*. (2012), Bisphenol A induces gene expression changes and proliferative effects through GPER in breast cancer cells and cancer -associated fibroblasts, *Environmental Health Perspectives*,**120**, 1177-1182.

Rochester , J. R., Bolden, A. L. (2015), Bisphenol S and F: A Systematic review and comparison of the hormonal activity of bisphenol A substitutes, *Environmental Health Perspectives*, **123**, 643-650.

Volmer, R., van der Ploeg, K., Ron, D. (2013), Membrane lipid saturation activates endoplasmic reticulum unfolded protein response transducers through their transmembrane domains, *Proceedings of the National Academy of Sciences*, **110**, 4628-4633.

Weigelt, B., Peterse, J. L., van't Veer, L. J. (2005), Breast cancer metastasıs: markers and models, *Nature Reviews Cancer*, **5**, 591-602.

Wang, J. N., Qiu, S. L., Chen, S. M., Xiong, C. Q., *et al*. (20114), MALDI-TOF MS imaging of metabolites with a n-(1-naphthyl) ethylenediamine dihydrochloride matrix and its application to colorectal cancer liver metastasis, *Analytical Chemistry*, **87**, 422-430.

Electronic Supplementary Material

Liquid Chromatography-Mass Spectrometry-based Metabolomics and Lipidomics Reveal Toxicological Mechanism of Bisphenol F in Breast Cancer Xenografts

ZHAO C. [1, 2], XIE P. [3], SONG Y. [1], YANG T. [1], TANG Z. [1], XIANG L. [1], ZHAO H. [1], WANG H. [2], and CAI Z. [1, *]

[1]State Key Laboratory of Environmental and Biological Analysis, Department of Chemistry, Hong Kong Baptist University, Hong Kong SAR, China.

[2]State Key Laboratory of Environmental Chemistry and Ecotoxicology, Research Center for Eco-Environmental Sciences, Chinese Academy of Sciences, Beijing, China.

[3]Ministry of Education Key Laboratory of Analysis and Detection Technology for Food Safety, Fuzhou University, Fuzhou, China.

*corresponding author: CAI Z.

E-mail: zwcai@hkbu.edu.hk

Materials and Methods

Establishment of tumor nude mice model (Tumor xenografts) and BPF administration. Briefly, female BALB/c nude mice aged 4-weeks-old were obtained from HKCU and were maintained in sterile individually ventilated cages (IVC) under the following conditions: 20 ± 2 ^{o}C of temperature, 45 ± 10% of relative humidity with a 12-h light/dark cycle in each day. After 7 days of adaptation period, 1×10^{6} of MDA-MB-231 (Epidermal growth factor receptor, EGFR positive) were subcutaneously implanted into the armpit of each mouse. The diameters of tumor were measured by using caliper assessment every week, and were allowed to grow for 14 days. Female nude mice were randomly divided into three groups (n=6 for each) including control group (olive oil), BPA-treated group (100 μg /kg body weight/day) and BPF-treated group (100 μg /kg/ day). All mice were treated by gastric infusion method with a dosage of BPA or BPF in olive oil once daily. The tumor volume was calculated by formula: L (tumor length) ×w (width) ×d (depth) × (π/6). The body weight of mice was measured every week, and the physical state was monitored every 4 days. After 56 days consecutive administration of BPF or BPA, the mice were sacrificed and the tissues were collected for omics analysis by using LC-MS and MALDI-IMS. For *in vivo* imaging of mice model, IRdye 800CW-EGF (Li-Cor Biosciences, Lincoln, Nebraska) was dissolved in the methanol at 5.0 mg/mL and was injected intravenously into the tail vein of nude mice after BPA/BPF treatment. After 4 days of dye injection, near-infrared optical imaging of nude mice was analyzed using the Odyssey CLx infrared imaging system (LI-COR Biosciences-US, Lincoln, NE) with a 800-nm fluorescence signal channel. Regions of interest (ROI) from control and treated group were selected to cover the whole mice and quantified with Image Studio Version 5.2 software (LI-COR Biosciences-US, Lincoln, NE).

Metabolite extraction from tissue. Tissue samples were dissected from control and BPF or BPA-treated group, and were washed with PBS, quick-frozen with liquid nitrogen. Tissues were stored at -80 ^{o}C prior to metabolites extraction. Fifty mg of tissue samples were homogenized using a Polytron PT2100 homogenizer (Kinematica, Lucerne, Switzerland) in 600 μL of ice-cold methanol and 150 μL of water, and then 450 μL of chloroform was added, homogenate was vortexed for 30 min at the 3,400 rpm on ice, 150 μL water was added to promote phase separation. The homogenate was again vortexed for 1 min and allowed to equilibrate at room temperature for 5 min. The mixture was centrifuged at 12,000 g for 15 min at -6 ^{o}C. The up and bottom layers were collected and transferred to another 1.5 mL-tube and dried in a freeze-dryer, respectively.

The LC-MS/MS-based global metabolomics, quantitative analysis of extracted proteins and data processing were also carried out as described in Zhao *et al*. (2017).

References

Zhao, C., Tang, Z., Yan, J. C., Fang, J., Wang, H. L., Cai, Z. W. (2017), Bisphenol S exposure modulate macrophage phenotype as defined by cytokines profiling, global metabolomics and lipidomics analysis, *Science of the Total Environment*, in press.

Figure S1. Effects of BPF and BPA in MDA-MB-231 tumor-implanted athymic BALB/c nude mice. (A) *In vivo* near-infrared optical imaging using IRdye 800CW-epidermal growth factor dye in the control (olive oil), 100 μg/kg/day BPF- and 100 μg/kg/day BPA-tread group. White circle indicate the location of breast tumor. Tumor volume (B) and tumor weight (C) were significantly increased in BPF- and BPA-treated groups compared with control (the symbol represents statistical significance between treated group and control group: * $P < 0.05$, ** $P < 0.01$; the same as below).

(A)

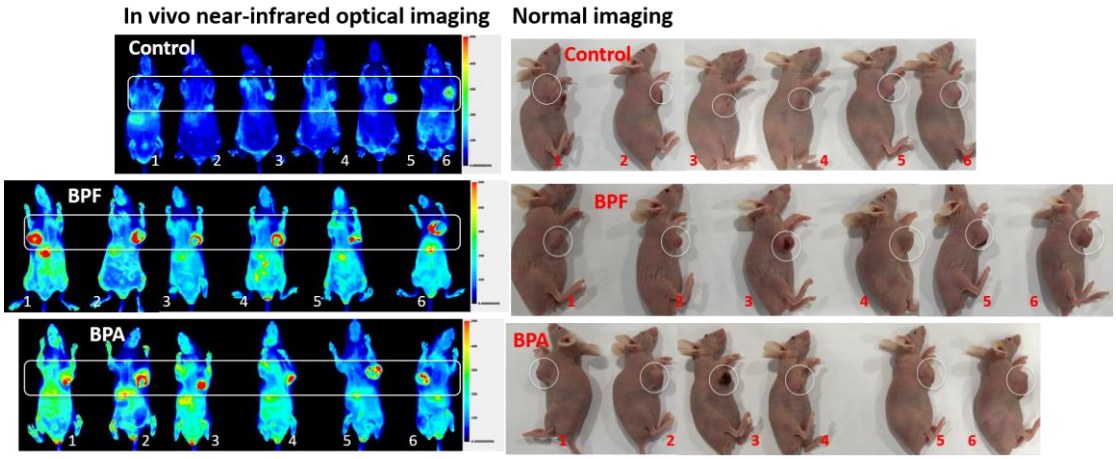

(B) (C)

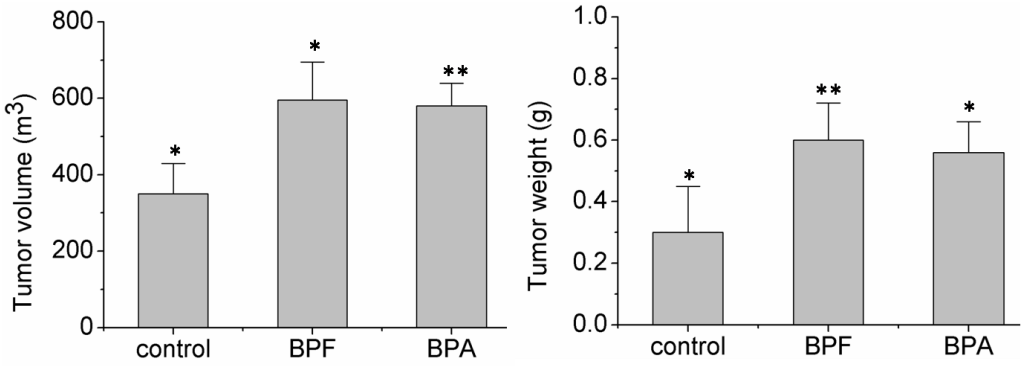

Figure S2. Two-dimensional PLS-DA score plots of kidney extract in the control group (red) and the BPF-treated group (black) (n=5) in positive and negative ionization mode. Metabolomics analysis on positive ionization mode (A) and negative mode (B); Lipidomics analysis on positive mode (C) and negative mode (D).

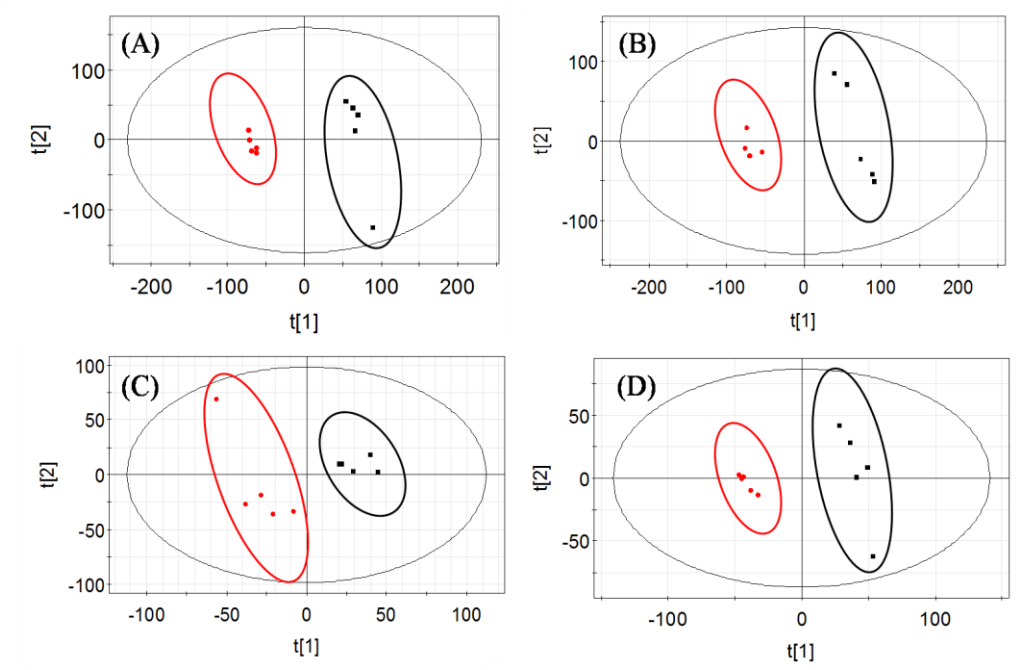
(A)
(B)
(C)
(D)
t[1]
t[2]

Table S1. Effects of BPF on gene expression in 100 μg/kg body weight/day BPF-treated kidney and liver.

Metabolic Pathways	Gene	Gene Expression Fold			
		In kidney /Control		In liver/Control	
		P	Fold	P	Fold
GSH biosysnthesis	Gss	0.05	0.9	0.12	0.1
	Ggt	0.01	0.3	0.09	0.1
	Gls2	0.12	0.4	0.12	0.5
Glycolysis	Ldha	0.21	1.4	0.03	1.6
	Phgdh	0.02	2.1	0.02	2.2
	HK	0.01	2.1	0.05	2.6
	Pkm2	0.05	1.2	0.12	1.6
Biosynthesis and degradation of GPs and GLs	Ccpt	0.11	3.2	0.02	1.2
	Dgat	0.32	2.6	0.01	1.0
	PIs	0.01	3.6	0.03	0.9
	Pla2g2a	0.01	0.4	0.12	0.1
	Pla2g12a	0.03	0.3	0.03	0.3

Table S2. Endogenous differential metabolites and lipids induced by BPF exposure in kidney and liver of breast cancer xenografts. Positive and negative ionization modes were represented by "P" and "N", respectively.

No.	Compounds	m/z	R.T.	Errors (ppm)	Ion mode	Related pathway
1	Glycine	75.9866	1.12	0	P	GSH biosysnthesis
2	Serine	105.0926	2.34	0	P	
3	Cysteine	122.0580	2.13	1	P	
4	GSH	308.0911	1.52	0	N	
5	Lactate	90.9979	1.54	1	N	Glycolysis
6	Pyruvate	88.9821	1.43	0	N	
7	G-6P	261.0558	2.12	0	N	
8	PC(20:4/22:6)	853.5622	15.43	1	P+N	Biosynthesis and degradation of GPs and GLs
9	PC(22:6/13:1)	761.4996	14.21	1	P+N	
10	PC(18:1/24:6)	859.6091	17.82	1	P+N	
11	PC(16:0p/22:4)	793.5985	18.21	1	P+N	
12	LPC(30:0)	691.5516	4.65	1	P+N	
13	LPC(20:0)	551.3951	5.11	1	P+N	
14	LPC(32:0)	719.5829	5.91	1	P+N	
15	PE(18:0p/22:6)	775.5516	15.41	1	P+N	
16	PE(18:1p/24:1)	811.6455	12.99	0	P+N	
17	PE(16:0/22:6)	763.5152	14.81	1	P+N	
18	LPE(33:4)	683.489	4.98	0	P+N	
19	LPE(33:5)	681.4733	4.01	0	P+N	
20	DAG(26:1/18:1)	732.6632	12.76	0	P+N	
21	DAG(19:1/16:0)	608.538	13.78	0	P+N	
22	DAG(16:1/18:1)	592.5067	15.33	1	P+N	
23	DAG(26:6/18:0)	724.6006	12.65	1	P+N	
24	DAG(38:4e)	630.5587	14.56	1	P+N	
25	TAG(16:0/16:0/24:0)	918.8615	20.11	1	P+N	
26	TAG(18:0/14:0/16:0)	806.7363	20.18	1	P+N	
27	TAG(18:0/20:1/22:4)	964.8459	21.92	1	P+N	

28	TAG(16:0e/22:5/24:1)	976.8823	23.19	0	P+N	
29	TAG(20:1/18:1/20:2)	938.8302	20.12	0	P+N	
30	TAG(15:1/18:0/19:0)	860.7833	21.02	0	P+N	
31	TAG(18:0e/18:0/20:4)	896.8197	21.60	0	P+N	
32	PI(16:0e/20:4)	844.5466	12.54	1	P+N	
33	PI (18:0/20:4)	886.5571	11.76	1	P+N	
34	PI(18:0/20:3)	888.5728	11.45	1	P+N	
35	PI(18:0/22:6)	910.5571	12.31	0	P+N	
36	PI(18:2/20:4)	882.5258	12.87	1	P+N	